A Test for the Zero Mean Hypothesis in Cosmology

Kiyotomo Ichiki[1, 2, *]

[1]*Kobayashi-Maskawa Institute for the Origin of Particles and the Universe, Nagoya University, Chikusa-ku, Nagoya, 464-8602, Japan*
[2]*Department of Physics and Astrophysics, Nagoya University, Nagoya 464-8602, Japan*

(Dated: December 9, 2014)

One working hypothesis on which analyses of cosmological data are based is the zero ensemble mean hypothesis, which is related to the statistical homogeneity of cosmological perturbations. This hypothesis, however, should be tested by observational data in the current era of precision cosmology. Herein, we test the hypothesis by analyzing recent, foreground-reduced cosmic microwave background (CMB) maps, combining the spherical harmonic coefficients of the masked CMB temperature anisotropies in such a way that the combined variables can be treated as statistically independent samples. We find evidence against the zero mean hypothesis in two particular ranges of multipoles, with significance levels of 2.5σ and 3.1σ in the multipole ranges of $\ell \approx 61$-86 and 213-256, respectively, for both the Planck and Wilkinson Microwave Anisotropy Probe maps. The latter signal is consistent with our previous result found by using brute-force Monte-Carlo simulations. However, within the method employed in this paper we conclude that the zero mean hypothesis is consistent with the current CMB data on the basis of Stouffer's weighted Z statistics, which takes multiple testing into account.

PACS numbers: 98.70.Vc, 95.30.-k, 98.80.Es

arXiv:1406.7613v3 [astro-ph.CO] 8 Dec 2014

I. INTRODUCTION

Recent precise measurements of anisotropies of the cosmic microwave background (CMB) as well as a number of probes of the large scale structure (LSS) of the universe have led us to the standard, concordant model of cosmology. In the standard cosmological model, the universe contains small density fluctuations on top of otherwise flat, homogeneous, and isotropic space-time. The density fluctuations are thought to be generated through quantum fluctuations in the accelerating expansion phase in the early universe, i.e., inflation. An important diagnostic characteristic of inflation models is that they predict statistically homogeneous and isotropic Gaussian fluctuations with a near scale-invariant power spectrum (for a review, see [1]).

Among these features, the Gaussianity and approximate scale invariance have been intensively tested by a number of observations and verified with high significance [2–5], while the statistical homogeneity and isotropy have been less tested and often assumed implicitly in cosmological analyses [6]. Recently, the test of statistical isotropy has attracted much attention [7–11], after the authors of [8] found hints for the breaking of statistical isotropy in the Wilkinson Microwave Anisotropy Probe (WMAP) CMB anisotropy data (see also, [12, 13]). The existence of the statistical anisotropy has been confirmed by Planck data [14], and more recently Akrami et al. have found the statistical anisotropy at the 3.3σ level by measuring the local variance, using the 1000 available Planck Full Focal Plane simulations [15]. On the other hand, no evidence has been found in a sample of luminous red galaxies observed by the Sloan Digital Sky Survey [16].

In this paper, we test statistical homogeneity using recent fullsky CMB temperature maps provided by the WMAP and Planck satellites. Specifically, we test the null hypothesis that the means of cosmological perturbations are zero in spherical harmonic space, which corresponds to the usual Fourier space in three-dimensional space. It is understood that the zero mean hypothesis is related to statistical homogeneity as follows [17]. We usually assume that because of the cosmological principle, perturbation variables, such as the CMB temperature, can be decomposed into a space-independent background value and perturbations, as $T = T_0(t) + \delta T(t, \vec{x})$ with

$$\langle \delta T(t, \vec{x}) \rangle = 0 \ , \tag{1}$$

where the angle brackets denote an ensemble average. Note that this decomposition can be done only if the expectation value of T is constant, i.e., $\langle T(t, \vec{x}) \rangle = $ const. with fixed time. It is always possible to satisfy Eq. (1) even if the expectation is not constant, but in that case the background temperature cannot be space-independent. The

*Electronic address: ichiki@a.phys.nagoya-u.ac.jp

condition that this expectation value is constant is equivalent to the statistically homogeneous (stationary) condition of the mean,

$$\langle \delta T(t,\vec{x})\rangle = \left\langle \delta T(t,\vec{x}+\vec{X})\right\rangle \qquad \forall \vec{X}\in R^3 \ , \tag{2}$$

where the time coordinate t is defined for the background temperature T to be homogeneous. Hence the zero mean hypothesis is equivalent to the statistical homogeneity of the mean. The temperature anisotropy can be written, in the linearized theory, as

$$\delta T(\vec{x},\hat{n},t) = \int \frac{d^3k}{(2\pi)^3}\mathcal{T}(\vec{k},\hat{n})\phi(\vec{k})e^{i\vec{k}\cdot\vec{x}} \ , \tag{3}$$

where $\phi(\vec{k})$ are the Fourier modes of the initial density perturbations and $\mathcal{T}(\vec{k},\hat{n})$ is the linear transfer function that relates the initial density perturbations to the currently observed temperature anisotropies. Because the temperature fluctuations are observed on the sphere, it is common practice to express them with real spherical harmonic coefficients

$$a_{\ell m}(\vec{x}) = \int d^2\hat{n}\delta T(\vec{x},\hat{n},t)R_{\ell m}(\hat{n}) \ , \tag{4}$$

where $R_{\ell m}$ is the real set of spherical harmonics. Because the transfer function in Eq. (3) is completely determined by the cosmological perturbation theory given a cosmological model, the zero mean condition $\langle \delta T(t,\vec{x})\rangle = 0$ is equivalent to the conditions $\left\langle \phi(\vec{k})\right\rangle = \langle a_{\ell m}(\vec{x})\rangle = 0$. In the following, we test whether the condition $\langle a_{\ell m}\rangle = 0$ is satisfied using the latest CMB data, replacing the ensemble average with the directional average assuming the statistical homogeneity and isotropy in the mean.

Studies on the zero mean hypothesis using CMB data can be found in Refs. [17] and [18]. One complication when testing the zero mean hypothesis with CMB data is the existence of the mask, which suppresses foreground contamination but generates correlations between the samples. Picon analyzed CMB data by constructing v-vectors that disentangle the correlations [17], while Kashino et al. utilized Monte-Calro simulations to take into account the correlations in the samples [18]. In this paper we build on the work of [17], and extend the analysis toward higher multipoles using the latest CMB data from Planck.

To assess any statistical properties of the foreground-reduced CMB maps strictly, one needs to use specific simulations. These simulations directly reflect uncertainties in the foreground cleaning methods, residuals of the antenna beam shape, anisotropy of the noise and others [7]. For the Planck experiment, we adopt hundred CMB and noise simulations produced by the Planck collaboration [33], and use these simulations to address these issues. In addition we compare the WMAP and Planck maps, which have different residuals of the antenna beam shape. We also compare the different foreground-reduced Planck maps, which have different uncertainties in the foreground cleaning methods. We will see that these maps give consistent results.

II. METHOD

Herein we summarize the method developed by [17]. Observed temperature fluctuations, $\delta T(\hat{n})_{\rm obs}$, involve a convolution with the detector beam window B and the pixel smoothing kernel K and can be expressed as

$$\delta T^{\rm obs}(\hat{n}) = M(\hat{n})\left(K * \left[B * \delta T^{\rm CMB}(\hat{n}) + N(\hat{n})\right]\right) \ , \tag{5}$$

where $\delta T_{\rm CMB}(\hat{n})$ is the CMB signal we want to estimate, $N(\hat{n})$ is instrument noise and $M(\hat{n})$ is the mask. Here we have omitted the foreground assuming that $M(\hat{n})$ can successfully mask the foreground contaminated regions. In spherical harmonic space, the above equation is expressed as

$$a^{\rm obs}_{\ell m} = \sum M_{\ell m;\ell' m'} a^{\rm full\,sky}_{\ell' m'} \ , \tag{6}$$

where $a^{\rm full\,sky}_{\ell m} = K_\ell B_\ell a^{\rm CMB}_{\ell m} + K_\ell n_{\ell m}$ consists of the spherical harmonic coefficients of the sky, including signal and noise, and $M_{\ell m;\ell' m'}$ is the mask-coupling matrix. Because instrumental noise is expected to be well described by a Gaussian distribution as shown in the WMAP [19] and Planck papers, ensemble averages of $a^{\rm obs}_{\ell m}$ are zero if those of $a^{\rm CMB}_{\ell m}$ are zero. Considering an axisymmetric mask that satisfies $M_{\ell m;\ell' m'} = M_{\ell m;\ell' m}\delta_{mm'}$ and using matrix notation for a fixed m, the above equation can be expressed as

$$\vec{a}^{\rm obs}_m = \boldsymbol{M}\cdot\vec{a}^{\rm full\,sky}_m \ , \tag{7}$$

where the dot represents inner product over multipoles ℓ. To remove the effect of the mask from the observed spherical harmonic coefficients and disentangle the coupling, consider m-independent v-vectors that satisfy the relation

$$\vec{v}^{\,t} = \vec{v}^{\,t}\boldsymbol{M} \ , \tag{8}$$

where

$$v_{\ell m} = \begin{cases} v_\ell & \text{for } |m| \le \ell_{\rm min} \text{ and } \ell_{\rm min} \le \ell \le \ell_{\rm max} \\ 0 & \text{(otherwise)} \ . \end{cases} \tag{9}$$

Let us construct a variable d_m as the dot product of $\vec{v}$ and $\vec{a}_m^{\rm obs}$

$$d_m \equiv \vec{v}^{\,t} \cdot \vec{a}^{\,\rm obs} = \vec{v}^{\,t}\boldsymbol{M}\vec{a}_m^{\,\rm full\,sky} = \vec{v}^{\,t} \cdot \vec{a}_m^{\,\rm full\,sky} \ , \tag{10}$$

for $|m| < m_{\rm max}$. The new stochastic variable d_m has the following properties:

1. Foreground insensitive, because we work on $a_{\ell m}^{\rm obs}$, the spherical harmonic coefficients of the masked sky
2. Statistically independent, because they are constructed as a linear combination of statistically independent variables $a_{\ell m}^{\rm CMB}$ and $n_{\ell m}$
3. Gaussian with zero mean, if $a_{\ell m}^{\rm CMB}$ and $n_{\ell m}$ are as well
4. Having m-independent variance, where $\sigma^2 = \sum_{\ell_{\rm min}}^{\ell_{\rm max}} K_\ell (B_\ell^2 C_\ell + N_\ell) v_\ell^2$.

Owing to these properties, we can formulate a simple statistical test of the zero mean hypothesis. In our test below, we estimate σ^2 directly from the data.

To obtain the v-vectors, it is convenient to work in pixel space. In pixel space, Eq.(8) is written as $(1 - M(\hat{n}))v(\hat{n}) = 0$. Substituting $v(\hat{n}) = \sum v_{\ell m} Y_{\ell m}(\hat{n})$ and defining the matrix

$$D_{i\ell} = (1 - M(\hat{n}_i)) \sum_{|m| \le \ell_{\rm min}} Y_{\ell m}(\hat{n}_i) \ , \tag{11}$$

where i runs over all pixels and $\ell_{\rm min} \le \ell \le \ell_{\rm max}$, we can rewrite the system of equations in Eq. (8) as

$$\boldsymbol{D}\vec{v} = 0 \ , \tag{12}$$

or, in component notation, $\sum_\ell D_{i\ell} v_\ell = 0$. The dimension of the matrix D is $(\ell_{\rm max} - \ell_{\rm min} + 1, N_{\rm pix})$, where we have used the Healpix pixelization scheme with $N_{\rm side} = 256$, and therefore $N_{\rm pix} = 786432$. We find an approximate solution of this system of equations using singular value decomposition (SVD). The SVD of the matrix D is expressed as

$$\boldsymbol{D} = \boldsymbol{U}\boldsymbol{\Sigma}\boldsymbol{V}^T \ , \tag{13}$$

where $\boldsymbol{U}\boldsymbol{U}^T = \boldsymbol{V}\boldsymbol{V}^T = \boldsymbol{I}$. The columns of $\boldsymbol{U}$ and $\boldsymbol{V}$ are orthogonal eigenvectors of $\boldsymbol{D}\boldsymbol{D}^T$ and $\boldsymbol{D}^T\boldsymbol{D}$, respectively, and $\boldsymbol{\Sigma}$ is a diagonal matrix containing the singular values of the matrix $\boldsymbol{D}$ in descending order. We choose the vector $\vec{v}$ to be the last right singular vector, so that

$$|\boldsymbol{D}\vec{v}|^2 = \Sigma_{\rm last}^2 \ . \tag{14}$$

The last singular value, $\Sigma_{\rm last}$, should be small but non-zero, and therefore our solution is only approximate. Following [17], we choose the binning of multipoles so that the last singular value divided by the norms of the mask and the sky encoded in $\vec{v}$ is sufficiently small ($\lesssim 10^{-8}$).

III. RESULT

A. test using a simple statistic

We tested the zero mean hypothesis with the stochastic variable d_m, which is constructed as a linear combination of $a_{\ell m}$ given by Eq. (10). To perform the inner product in Eq. (10), we divide the multipoles into bins [17], and the ranges of these bins are shown in Fig. 1. In the figure, we show histograms of the variable d_m, constructed from the

WMAP (red) and Planck (black) maps. The variable d_m is normalized by the sample variance σ. It is evident from the figure that in the examined multipole range the Planck and WMAP maps give consistent results. The means of the distributions are consistent with zero, except for possible deviations for the multipole ranges of $\ell \approx 61$ - 86 and $\ell \approx 213$ - 256.

In Fig. 2, we depict the result of the test showing how many sigmas the observed data deviate from the zero mean. Here we perform a simple test assuming Gaussian statistics as follows. We estimate the mean from the sample by computing $\bar{d} = \sum_m d_m/(2\ell_{\rm min}+1)$ and then obtain the error in the estimate of the mean from the formula

$$\sigma(\bar{d}) = \frac{\sigma}{\sqrt{2\ell_{\rm min}+1}} \ , \tag{15}$$

where $\sigma^2 \equiv \sum (d_m - \bar{d})^2/(2\ell_{\rm min})$ is the sample variance. The Z-scores in the figure are simply defined by $Z = \bar{d}/\sigma(\bar{d})$ for each multipole bin.

There are hints of deviations in the ranges around $\ell \approx 70$ and $\ell \approx 230$. Significance levels are 2.5σ for the former and 3.1σ for the latter. For the latter signal, the significance is slightly larger for the Planck map. The other multipole ranges are consistent with the zero mean hypothesis.

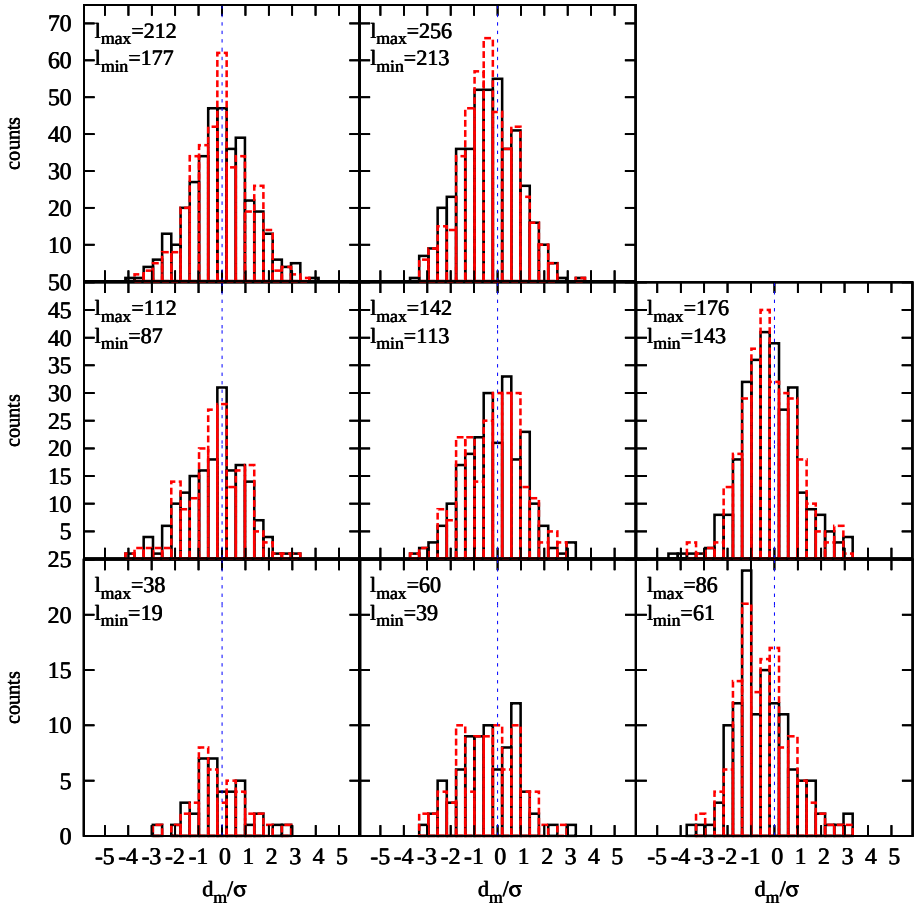

FIG. 1: Histograms of stochastic variable d_m normalized by the sample variance. Binning in ℓ space has been done and is shown in the figure. If the $a_{\ell m}$ of the CMB follow a Gaussian distribution with a zero mean, so does the variable d_m. The red histograms were obtained from the WMAP map, and the black from Planck map.

B. test using Planck simulations

In the simple test presented above we assume symmetric instrumental beams and isotropic noise. However, in actual experiments such as the WMAP and Planck ones, beams are not perfectly symmetric, and noise is anisotropic due to the scan strategy. In fact, asymmetric instrumental beams can introduce statistical artifacts (e.g., [20]), and anisotropic scan strategy can break the zero mean assumption in the noise. To see whether these effects change the results in the previous section, we adopt the hundred CMB and noise sky simulations produced by the Planck

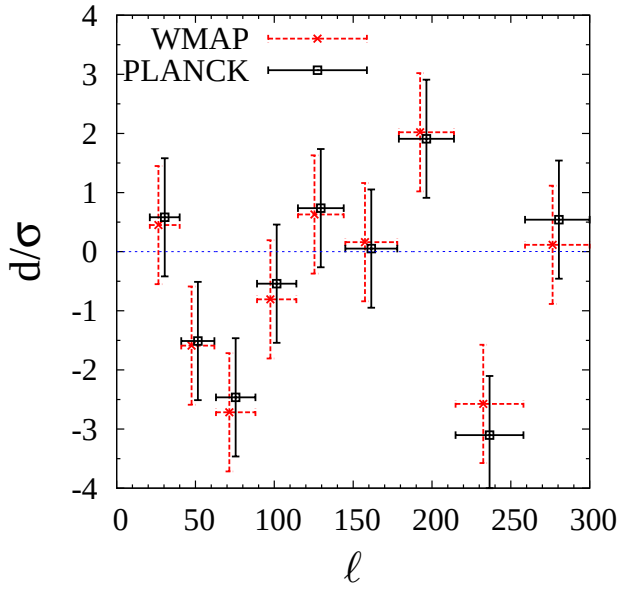

FIG. 2: Deviations from the zero mean hypothesis from WMAP nine-year data (red dashed) and Planck SMICA (black solid) maps. The vertical error bars are $\pm\sigma$, while the horizontal error bars are the width of the binning.

collaboration and apply the same method to these sky maps. In these simulations they have taken into account the scan strategy, the instrumental performance, and the noise property of the Planck experiment.

Figure 3 shows the histograms of the means using the hundred Planck simulations of CMB with noises at the 100 GHz and 143 GHz bands. The means of the simulations are shown to be consistent with the zero mean hypothesis, as shown in the right panel of Fig. 3. Again, we find the deviations in the multipole ranges around $\ell \approx 70$ and $\ell \approx 230$ significant. For the former, we find two samples that show larger deviations from zero than the actual Planck data, and for the latter, we find no sample out of the hundred simulations that shows the larger deviation. The p-values are summarized in table I.

bin		$\pm 20^\circ$ cut
$\ell_{\rm min}$	$\ell_{\rm max}$	Simulation
19	38	54%
39	60	6%
61	86	2%
87	112	61%
113	142	41%
143	176	96%
177	212	5%
213	256	<1%
256	300	58%

TABLE I: Probabilities of supporting the null hypothesis (p values) that the CMB fluctuations have a zero mean, using the hundred Planck sky simulations.

We should caution, however, that the simulations used here do not exactly correspond to the data we analyze, i.e. the SMICA map. Therefore, these simulations should be recognized as an estimate of Planck's instrumental effects in the SMICA map. Furthermore, while we find no sample out of the simulations that shows the larger deviation at the $213 \lesssim \ell \lesssim 256$ bin, one should use more simulations to confirm the significant detection.

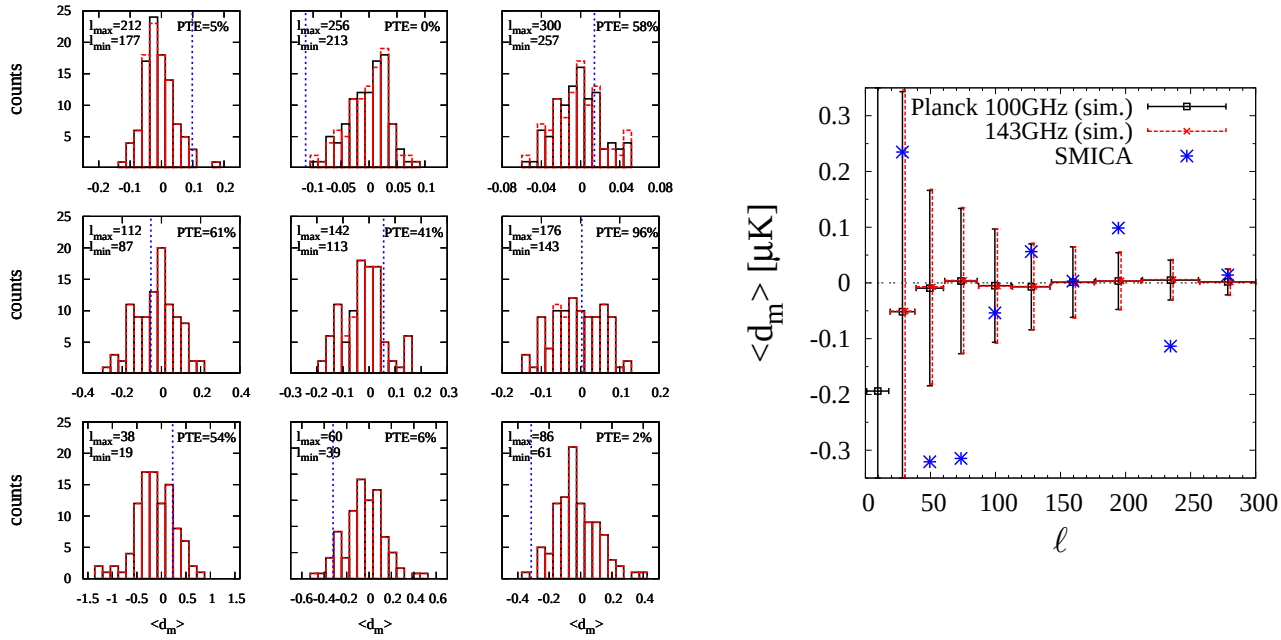

FIG. 3: Histograms (left) and plots (right) of the means $\langle d_m \rangle$ calculated using the Planck (CMB + Noise) simulations at the 100 GHz (black) and 143 GHz (red) bands. The means derived from the actual Planck SMICA map are shown as the blue dashed lines (left) and points (right). Probability to exceed (PTE) is also shown based on the simulations at the 100 GHz band.

IV. DISCUSSION

A. Instrument Noise

The formulation described in the previous section ignores the effect of the instrument noise. Although instrument noise that is expected to have a zero mean would not bias the test of the zero mean hypothesis, it degrades the statistical power. To demonstrate how the instrument noise of the WMAP and Planck could affect the test of the zero mean hypothesis, we construct the variable d_m from the expected noise values for the sky in the WMAP and Planck SMICA (Spectral Matching Independent Component Analysis) maps and show the results in Fig. 4 for the multipole range of $\ell \approx$ 213-256. As expected, the noise in the Planck map are negligibly small compared with the signal for this angular scale, because of its high angular resolution. On the other hand, noise can contribute up to 40% for the WMAP case, and this might be a reason for a smaller S/N from the WMAP than that from Planck at this scale (see Fig. 2). Thus we did not explore the test at smaller scales, $\ell \gtrsim 300$.

While the instrumental noise of the Planck satellite at angular scales considered here should be significantly lower than the CMB signal as shown in Fig. 4, that of the WMAP satellite begins to dominate at highest multipole bins and may bring unwanted statistical artifacts. Therefore, we make a simple test by simulating the anisotropic noise based on the hit counts of the WMAP observation. Specifically, we create hundred noise maps based on the hit count data of the WMAP W-band observation, apply the same method to the maps, and obtain the distributions of d_m of the WMAP anisotropic noise. In Fig. 5, we show the result of our hundred noise simulation of the WMAP anisotropic noise together with the actual data points. While, on large angular scales, the WMAP noise is negligibly small compared with the signal, they become comparable at the $257 \lesssim \ell \lesssim 300$ bin. Thus, as we discussed above, we did not explore the test at smaller scales, even though the WMAP noise is consistent with zero mean.

While anisotropic noise will have zero mean, the correlated noise in the time-ordered data could potentially violate the zero mean hypothesis to some extent, making striping artifacts in the map. However, because the effect will be different between WMAP and Planck, and therefore we expect that it is not a major concern given that the results from these two experiments agree.

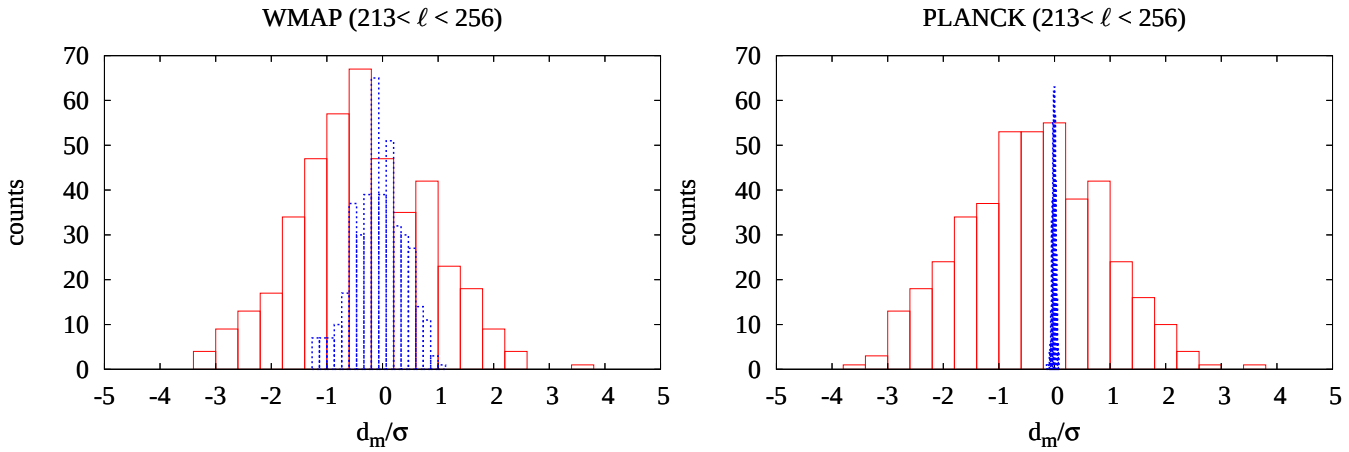

FIG. 4: Histograms of stochastic variable d_m from the signal plus noise (red; solid line) and expected noise only (blue; dashed line), normalized by the sample variance for the bin of $213 \leq \ell \leq 256$. The top panel is for the WMAP data and the bottom is for Planck (SMICA).

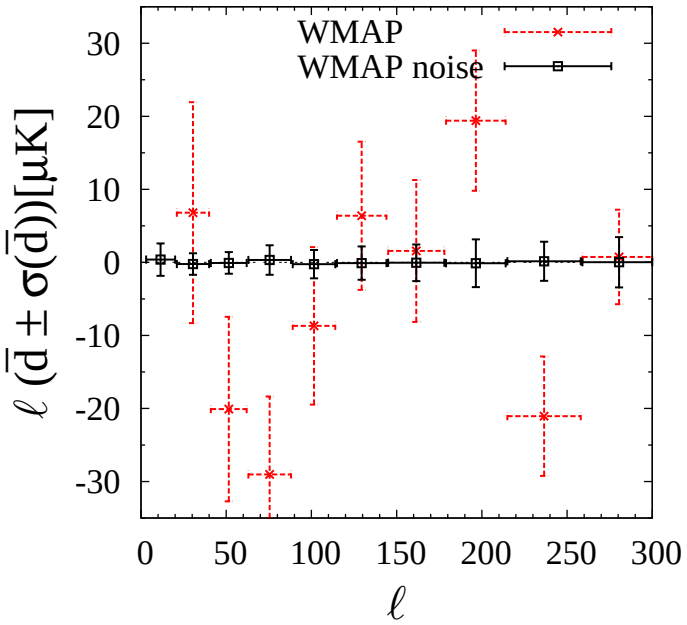

FIG. 5: Means of stochastic variable d_m from the simulations of the WMAP W-band noise (black), together with the actual WMAP data (red). The error bars are estimated from the hundred simulations for the anisotropic noise, and from the sample for the actual data. We multiply y-axis by ℓ for visualization purpose.

B. Foreground

Another issue we have to address is the foreground. One disadvantage of the simple and clear method described in this paper is that it must utilize an axisymmetric mask to simplify the convolution of the mask as in Eq. (7), while the foreground is, of course, not axisymmetric. We compare our axisymmetric mask with the ones used for the CMB power spectrum estimates of WMAP and Planck in Fig. 6. Although directions toward galactic disk where the cosmological CMB is heavily contaminated are removed by our axisymmetric mask, some parts of the sky at high galactic latitudes that are removed from the WMAP and Planck analyses are included in ours. To estimate how the foreground has contaminated the results in the previous section, we examine the same analysis but with more extensive and more aggressive masks that cut the region in the galactic latitude $|b| \leq 20^\circ \pm 5^\circ$. The results are shown in Fig. 7. Overall, we find mutually consistent results. In fact, for the eighth bin ($\ell \approx 213 - 256$), the significance remains the same even for $|b| \leq 25^\circ$ although the standard deviation σ becomes larger because of the smaller analyzed

bin		±20° cut			
$\ell_{\rm min}$	$\ell_{\rm max}$	SMICA	SEVEM	NILC	WMAP
19	38	56.1%	56.2%	56.3%	65.3%
39	60	13.1%	13.3%	13.2%	11.2%
61	86	1.38%	1.25%	1.14%	0.659%
87	112	58.8%	53.1%	53.6%	42.0%
113	142	46.2%	47.8%	47.8%	52.9%
143	176	95.8%	99.6%	99.7%	87.2%
177	212	5.61%	6.11%	6.13%	4.33%
213	256	0.192%	0.213%	0.175%	1.00%
256	300	58.8%	64.1%	63.1%	90.8%
Stouffer's Z		1.74	1.33	1.38	1.14 %

TABLE II: Probabilities of supporting the null hypothesis (p values) that the CMB fluctuations have a zero mean, for different maps.

bin		±15°	±20°	±25°
$\ell_{\rm min}$	$\ell_{\rm max}$		SMICA	
19	38	59.6%	56.1%	52.7%
39	60	13.1%	13.1%	12.9%
61	86	1.28%	1.38%	1.88%
87	112	63.8%	58.8%	51.6%
113	142	40.1%	46.2%	74.1%
143	176	99.7%	95.8%	92.0%
177	212	5.11%	5.61%	14.4%
213	256	0.511%	0.192%	0.193%
256	300	84.9%	58.8%	28.0%

TABLE III: Probabilities of supporting the null hypothesis (p values) that the CMB fluctuations have a zero mean, for different sky cuts.

sky area. This is consistent with what the previous work found with the WMAP seven-year map [18].

The same analysis is also done using other types of foreground-reduced maps from Planck as the SMICA map, namely, SEVEM (internal template fitting) and NILC (linear internal combination in a needlet space) maps. These maps are generated through processes completely different from those of SMICA maps and thus have different weights to both the frequencies and multipoles.

Table II and III summarize the probabilities of supporting the null hypothesis for different sky cuts and different foreground-reduced maps. We find that all the different foreground-reduced maps from Planck give consistent, almost indistinguishable results. The WMAP and Planck data are also consistent with each other, suggesting that instrumental and scanning effects that may cause apparent violations of statistical homogeneity are negligible. At the eighth bin ($\ell \approx 213$ - 256) the signal is slightly reduced for the WMAP map, but the small signal may be attributable to the instrument noise as discussed above. We also note that while the results in tables II and III are based on the simple equation (Eq. (15)), that in table I is derived directly from the histogram of Planck simulations, without assuming Gaussianity. The results in the tables clearly shows the same tendency.

Even though our result shows that the different foreground-reduced maps give consistent results, it does not necessarily mean that foreground contamination is not an issue, because these foreground subtraction methods are calibrated off the same Planck foreground model. To see how the foreground residuals could have an effect on the results, we do a few simple tests with varying amount of residual foreground contamination using the SMICA residual map at the HFI 100 GHz band, which is shown in Fig. 8. Foreground intensity of 100%, 10%, and 1% of the residual map are added to the SMICA CMB map and we apply the same method to the three maps. The result is shown in the left panel of Fig. 7. We find that our results are stable against the residual foreground contamination if the foreground residuals are less than 10%.

Another potential issue would be that the zero levels of temperature (i.e., monopoles) in the Planck experiment

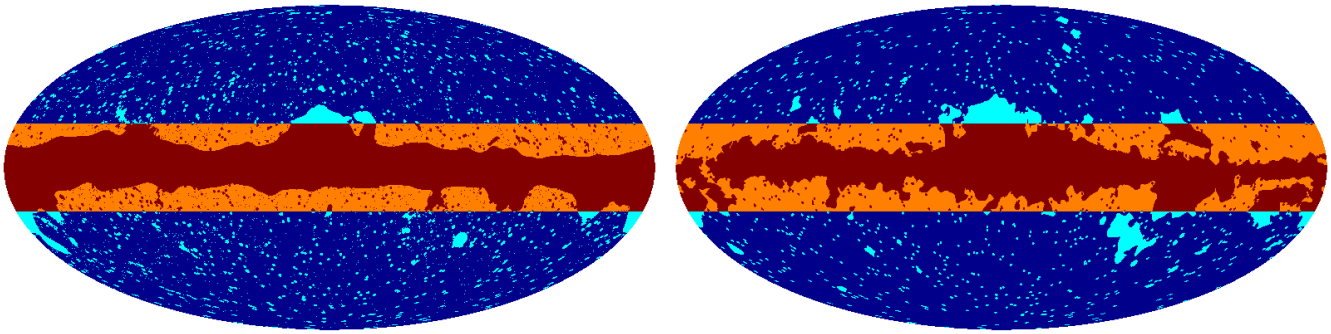

FIG. 6: Comparison of the masks used in this paper and cosmological analyses by the Planck (left) and WMAP (right) collaborations. The masked regions in the Planck and WMAP analyses are shown in cyan. Our axisymmetric mask is along the galactic plane and shown in orange.

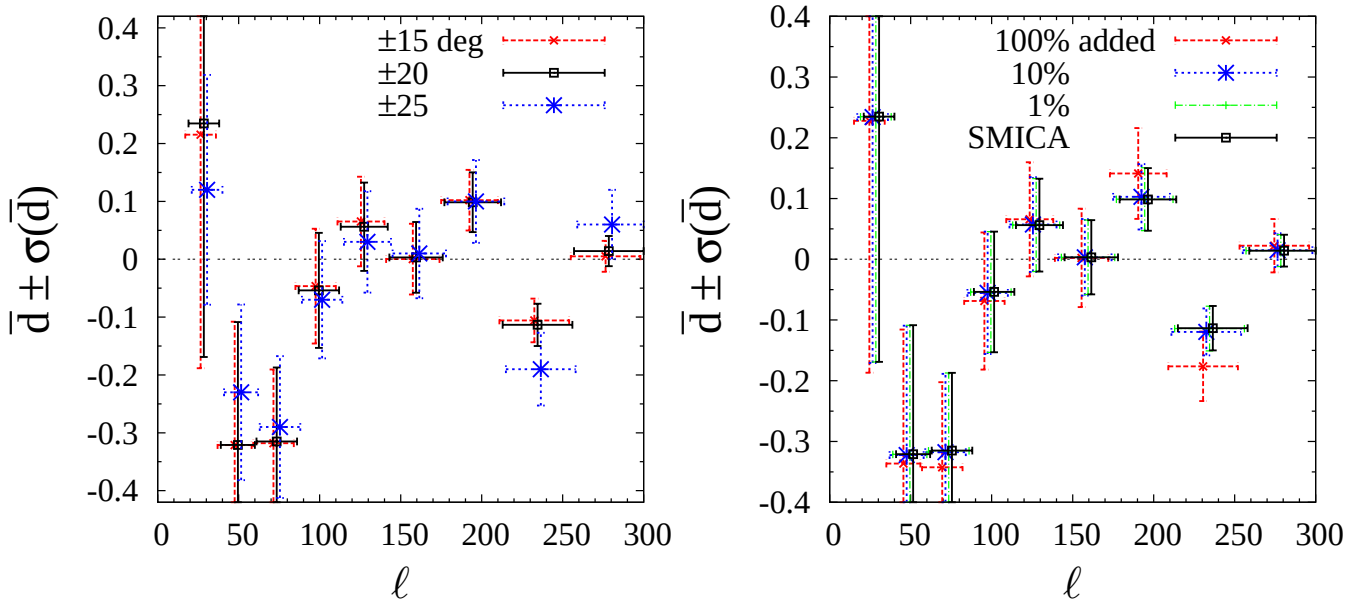

FIG. 7: Estimated means with error bars for different sky cuts (left) and with different foreground residuals (right) as indicated. In the figure we have not normalized by σ as it was done in Fig. 2. We have shifted the ℓ values by $+2$ for $|b| \leq 15^\circ$ and 10 % foreground cases, by -2 for $|b| \leq 25^\circ$ and 1 %, and by $+4$ for 100 % foreground case, for clarity.

are unconstrained. For example, as discussed in [21], the reported monopoles with uncertainties are -300.84 ± 2.23, -22.83 ± 0.78 and -28.09 ± 0.64 μK at the 30, 44, and 70 GHz bands, respectively. Because it is not trivial how the uncertainty in the monopole temperature affect the significance of the statistical inhomogeneity found at high multipole ranges, we do a simple test to check the effect. Specifically, we apply the same method to the map to which we add an additional monopole component with ± 10 μK, which is much larger than the uncertainty listed above. We found that the effect can be safely neglected for higher multipole regions considered in our analysis.

An analysis has been made in Kashino et al. [18], where we found an anomalously large deviation from the zero mean hypothesis at the multipole range $\ell \approx 221$ - 240 using Monte-Carlo simulations with the WMAP maps. The deviation was as large as 99.93% confidence level, regardless of the different frequency maps and different masks. The multipole ranges that show deviations from the zero mean hypothesis are consistent between Kashino et al. [18] and the results presented in this paper, although the methods used are completely independent from each other.

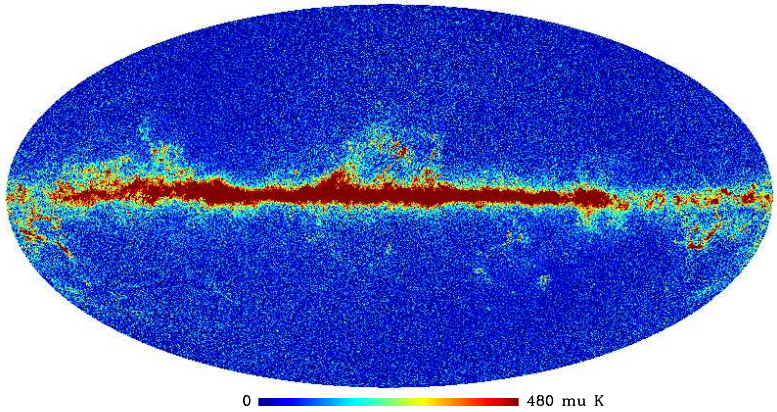

FIG. 8: The SMICA residual foreground map at the HFI 100GHz band.

C. Look-Elsewhere Effect

Finally, let us evaluate the significance as a whole to draw a conclusion against the null hypothesis. Because we have tested nine multipole bins for Planck maps (eight for the WMAP), we should take into account the effect whether apparent anomalies are found just because of statistical outliers. The effect is often called the look-elsewhere effect. In order to take this effect into account, we combine p-values by calculating the Stouffer's weighted Z (Liptak-Stouffer method), which is defined as [22]

$$Z \equiv \frac{\sum_1^n w_i Z_i}{\sqrt{\sum_1^n w_i^2}} \,. \tag{16}$$

Here Z_i is the so-called Z-score defined by $Z_i = \Phi^{-1}(1-p_i)$, where Φ is the standard normal cumulative distribution function and w_i is the number of degrees of freedom for the i-th bin. The combined variable Z, which follows the standard normal distribution if the common hypothesis is true, reflects the fact that we have done multiple tests for a common hypothesis. From the p-values listed in Table II, we find the values of Stouffer's weighted Z as

$$Z = 1.74 \text{ (SMICA)},\ 1.14 \text{ (WMAP)} \,, \tag{17}$$

which means, the percentages to reject the zero mean hypothesis are 91.8 % and 74.5 %, respectively. Therefore we may conclude that the zero mean hypothesis is consistent with observational data as a whole.

There is the possibility to perform additional tests to confirm whether or not the anomalous deviations from the zero mean hypothesis found here are just statistical fluctuations due to a particular realization of the Universe. A straightforward test is to make use of full-sky CMB polarization data that will soon be released from the Planck collaboration. Although the polarization anisotropies are made from common curvature fluctuations, their transfer functions do not completely coincide with those of temperature anisotropies, and thus they will lend additional statistical power. Another test is to look into large-scale structure data, which offers an independent probe for primordial fluctuations [23–25]. The comoving scale that corresponds to the multipole range of $\ell \approx 213$ - 256 is approximately $k \approx 0.015$ - 0.018 Mpc^{-1}, which is at the edge of the current galaxy survey by BOSS [26] and will be within reach in future galaxy surveys, such as Euclid [27], LSST [28], SKA [34] and others. Interesting ideas have been discussed in Refs. [24, 29–32], which include arguments that cosmic star formation histories and the kinetic Sunyaev-Zel'dovich effect can be used to probe inside our past light cone and thus they become powerful tools to probe into the cosmic homogeneity.

Before concluding, we would like to comment on the connection with studies on non-Gaussianity in the CMB. In analyses of higher-order statistics, such as the bispectrum, the zero mean condition has been implicitly assumed and one estimates a correlation of the form $\langle a_{\ell m} a_{\ell' m'} a_{\ell'' m''} \rangle$. Consider a case where the mean of $a_{\ell m}$ was not zero but the bispectrum was zero around the mean; it is expected that the three point correlation of the above form would have an amplitude on the order of

$$\langle a_{\ell m} a_{\ell' m'} a_{\ell'' m''} \rangle \sim C_\ell \, \langle a_{\ell m} \rangle \,. \tag{18}$$

Therefore, constraints on non-Gaussianity using the bispectrum in the literature could be used to put constraints on the mean of the spherical harmonic coefficients when this is the case.

V. CONCLUSION

We have tested one working cosmological hypothesis, which states that cosmological perturbations have a zero ensemble mean, using the latest CMB temperature anisotropy maps from the WMAP and Planck satellites. We find evidence against the zero mean hypothesis in two particular ranges of multipoles, with significance levels of 2.5σ at $\ell \approx 61$ - 86 and 3.1σ at $\ell \approx 213$ - 256. However, in the present analysis, we conclude that the zero mean hypothesis is consistent with the current observational data on the basis of the Stouffer's weighted-Z statistics, which takes into account multiple testing. The zero mean hypothesis can be further tested by future CMB polarization data that will be available soon from Planck satellite.

Acknowledgments

The author would like to thank T. T. Takeuchi, D. Kashino, M. Sasaki, T. Tanaka, M. Butcher, and A. Taruya for useful discussions especially at the Mini-workshop on Gravitation and Cosmology for APC-YITP collaboration. Thanks also go to the anonymous referees for giving us helpful and valuable comments. This work has been supported in part by Grant-in-Aid for Scientific Research No. 24340048 from the Ministry of Education, Sports, Science and Technology (MEXT) of Japan.

[1] D. Baumann, ArXiv e-prints (2009), 0907.5424.
[2] Planck Collaboration, P. A. R. Ade, N. Aghanim, C. Armitage-Caplan, M. Arnaud, M. Ashdown, F. Atrio-Barandela, J. Aumont, C. Baccigalupi, A. J. Banday, et al., ArXiv e-prints (2013), 1303.5076.
[3] Planck Collaboration, P. A. R. Ade, N. Aghanim, C. Armitage-Caplan, M. Arnaud, M. Ashdown, F. Atrio-Barandela, J. Aumont, C. Baccigalupi, A. J. Banday, et al., ArXiv e-prints (2013), 1303.5084.
[4] Planck Collaboration, P. A. R. Ade, N. Aghanim, C. Armitage-Caplan, M. Arnaud, M. Ashdown, F. Atrio-Barandela, J. Aumont, C. Baccigalupi, A. J. Banday, et al., ArXiv e-prints (2013), 1303.5082.
[5] G. Hinshaw, D. Larson, E. Komatsu, D. N. Spergel, C. L. Bennett, J. Dunkley, M. R. Nolta, M. Halpern, R. S. Hill, N. Odegard, et al., ApJS **208**, 19 (2013), 1212.5226.
[6] R. Maartens, Royal Society of London Philosophical Transactions Series A **369**, 5115 (2011), 1104.1300.
[7] C.-G. Park, MNRAS **349**, 313 (2004), astro-ph/0307469.
[8] H. K. Eriksen, F. K. Hansen, A. J. Banday, K. M. Górski, and P. B. Lilje, ApJ **605**, 14 (2004), arXiv:astro-ph/0307507.
[9] J. Hoftuft, H. K. Eriksen, A. J. Banday, K. M. Górski, F. K. Hansen, and P. B. Lilje, ApJ **699**, 985 (2009), 0903.1229.
[10] F. K. Hansen, A. J. Banday, K. M. Górski, H. K. Eriksen, and P. B. Lilje, ApJ **704**, 1448 (2009), 0812.3795.
[11] A. Bernui, Phys. Rev. D **78**, 063531 (2008), 0809.0934.
[12] H. K. Eriksen, A. J. Banday, K. M. Górski, F. K. Hansen, and P. B. Lilje, ApJ **660**, L81 (2007), astro-ph/0701089.
[13] M. Axelsson, Y. Fantaye, F. K. Hansen, A. J. Banday, H. K. Eriksen, and K. M. Gorski, ApJ **773**, L3 (2013), 1303.5371.
[14] Planck Collaboration, P. A. R. Ade, N. Aghanim, C. Armitage-Caplan, M. Arnaud, M. Ashdown, F. Atrio-Barandela, J. Aumont, C. Baccigalupi, A. J. Banday, et al., ArXiv e-prints (2013), 1303.5083.
[15] Y. Akrami, Y. Fantaye, A. Shafieloo, H. K. Eriksen, F. K. Hansen, A. J. Banday, and K. M. Górski, ApJ **784**, L42 (2014), 1402.0870.
[16] A. R. Pullen and C. M. Hirata, J. Cosmology Astropart. Phys. **5**, 027 (2010), 1003.0673.
[17] C. Armendariz-Picon, JCAP **3**, 48 (2011), 1012.2849.
[18] D. Kashino, K. Ichiki, and T. T. Takeuchi, Phys. Rev. D **85**, 063001 (2012), 1112.0924.
[19] N. Jarosik, C. L. Bennett, J. Dunkley, B. Gold, M. R. Greason, M. Halpern, R. S. Hill, G. Hinshaw, A. Kogut, E. Komatsu, et al., ApJS **192**, 14 (2011), 1001.4744.
[20] I. K. Wehus, L. Ackerman, H. K. Eriksen, and N. E. Groeneboom, ApJ **707**, 343 (2009), 0904.3998.
[21] Planck Collaboration, N. Aghanim, C. Armitage-Caplan, M. Arnaud, M. Ashdown, F. Atrio-Barandela, J. Aumont, C. Baccigalupi, A. J. Banday, R. B. Barreiro, et al., ArXiv e-prints (2013), 1303.5066.
[22] M. C. Whitlock, Journal of Evolutionary Biology, **18**, 5 (2005).
[23] F. Sylos Labini, Classical and Quantum Gravity **28**, 164003 (2011), 1103.5974.
[24] B. Hoyle, R. Tojeiro, R. Jimenez, A. Heavens, C. Clarkson, and R. Maartens, ApJ **762**, L9 (2013), 1209.6181.
[25] B. Pandey, MNRAS **430**, 3376 (2013), 1301.4961.
[26] F. Beutler, S. Saito, H.-J. Seo, J. Brinkmann, K. S. Dawson, D. J. Eisenstein, A. Font-Ribera, S. Ho, C. K. McBride, F. Montesano, et al., ArXiv e-prints (2013), 1312.4611.
[27] R. Laureijs, J. Amiaux, S. Arduini, J. . Augueres, J. Brinchmann, R. Cole, M. Cropper, C. Dabin, L. Duvet, A. Ealet, et al., ArXiv e-prints (2011), 1110.3193.
[28] LSST Science Collaboration, P. A. Abell, J. Allison, S. F. Anderson, J. R. Andrew, J. R. P. Angel, L. Armus, D. Arnett, S. J. Asztalos, T. S. Axelrod, et al., ArXiv e-prints (2009), 0912.0201.

[29] A. F. Heavens, R. Jimenez, and R. Maartens, J. Cosmology Astropart. Phys. **9**, 035 (2011), 1107.5910.
[30] J. Goodman, Phys. Rev. D **52**, 1821 (1995), astro-ph/9506068.
[31] R. R. Caldwell and A. Stebbins, Physical Review Letters **100**, 191302 (2008), 0711.3459.
[32] T. Clifton, C. Clarkson, and P. Bull, Physical Review Letters **109**, 051303 (2012), 1111.3794.
[33] http://wiki.cosmos.esa.int/planckpla/index.php/Simulation_data
[34] https://www.skatelescope.org